Dalton Transactions

ROYAL SOCIETY OF CHEMISTRY

PAPER

View Article Online
View Journal

Cite this: DOI: 10.1039/d6dt00524a

Synthesis, structure & diphenylacetylene reduction reactivity of a carbide-supported Fe_4Mo_2 carbonyl cluster: a higher Fe-valence hydride intermediate for enhanced selectivity

Emily Dick, † Chris Joseph, † Vincent M. Lynch and Michael J. Rose *

The novel four-iron, two-molybdenum cluster $[(\mu_6\text{-C})Fe_4Mo_2(CO)_{18}]^{2-}$ (**2**) containing an interstitial carbide has been structurally characterized and prepared from the corresponding Fe_4 dianion $[(\mu_4\text{-C})Fe_4(CO)_{12}]^{2-}$ (**1**) supported by two crowned alkali units in $[K(benzo\text{-}18\text{-}crown\text{-}6)]^+$. In the X-ray structure of **2**, the two molybdenum atoms share an internal geometry of a *cis* orientation about the central carbide, which indicates the stability of the well-known 'butterfly' Fe_4C core found in the precursor **1**, and this finding is consistent with other bis-heterometal variants of general formula $[Fe_4M_2]$ (M = Ni, Cu, Rh, Au). Reactivity studies monitoring the reduction of diphenylacetylene (DPA) catalyzed by **2** showed selective reduction to *cis*-diphenylethylene. The effect of proton source pK_a and steric bulk on DPA reduction demonstrated that product selectivity is enhanced with increased steric bulk near the protonation site, and that conversion increases with more acidic proton sources. Overall, increased selectivity is observed with **2** compared with catalyst-free reactions, Fe-only clusters and the Fe_5Mo variant. We attribute the beneficial reactivity profile of cluster **2** to the electronic effect of the two Mo(0) centers, which lead to higher valent iron sites in the hydride intermediate cluster(s), thus decreasing non-specific reduction and increasing selectivity.

Received 3rd March 2026,
Accepted 30th April 2026

DOI: 10.1039/d6dt00524a

rsc.li/dalton

Introduction

Renewed interest in iron-carbide clusters in the last decade has spurred the development of heterometal congeners of such clusters, which may prove useful as a means of providing access to higher valent clusters while maintaining the interstitial carbide. Such clusters have found utility as catalysts in Fischer–Tropsch,[1] H_2 splitting and proton reduction[2–5] as well as CO and CO_2 reduction.[6,7] Additionally, structural relevance to the six-coordinate carbide of nitrogenase led DeBeer *et al.* to conduct X-ray emission studies that provided insight into the electronic structure of the delocalized orbitals of the iron-carbide core.[5,8,9] Research into converting bound carbon-based ligands (CO, CS_2, CN) or carbon-based electrophiles (CS, CI_4, CH_2I_2, CF_2Br_2 *etc.*) to a carbide unit has thus far proven unfruitful – our work included[10] – and thus developing a fundamental understanding of carbide as a ligand as yet remains in the family of organometallic, low-valent metal carbonyl clusters – some with bio-relevant metals (from nitrogenase: namely Fe, Mo and V).

Since the report of the first tetra-iron-carbide cluster $[Fe_4(\mu_4\text{-}C(COOMe))(CO)_{12}]^-$,[11] the 'open-face' carbide cluster has demonstrated increased reactivity compared with its more 'closed' penta- and hexa-iron counterparts, thus serving as a useful synthon for the development of heterometal clusters.[3,12–14] A survey of the Cambridge Crystallographic Data Center (CCDC) reveals a number of published Fe_4M_2 clusters (M = d block metal) largely based upon heterometal addition to the tetra-iron-carbide cluster $[Fe_4(\mu_4\text{-C})(CO)_{12}]^{2-}$ and the analogous penta-iron-carbide cluster, or alternatively heterometal substitution of hexa-iron-carbide clusters. Regarding 3d metals, reports employing copper as the heterometal demonstrate the utility of a variety of copper-ligand motifs. The limited number of structures containing any d block heterometal (only Ni, Cu, Rh, Au), however, indicate limited synthetic investigations and provide an opportunity for further investigation.[15–19] The Fe_4M_2 clusters bear a variety of alternative non-CO ligands, including halides, phosphines and nitriles. The oxidation state of such clusters ranges from 0 to −2 with the cluster $[Fe_4(\mu_6\text{-C})(CO)_{14}(CuCl)_2]^{2-}$ exhibiting the highest average metal oxidation state of +1.[17]

Our group has examined ligand substitutions of the well-characterized Fe_6 clusters to understand the reactivity of hex-

The University of Texas at Austin, Austin, TX 78757, USA.
E-mail: mrose@cm.utexas.edu
† Equal author contribution.

airon-carbide clusters. Previous work has explored the substitution of electrophilic sulfur sources (S_2Cl_2 and S_8) and thiolate (PhS-Cl) on Fe_6^{2-} clusters, thus affording the first reported thiolato-iron-carbide complex.[20] We also demonstrated that by using *in situ* oxidation, reactive, polyhedral skeletal electron pair theory (PSEPT)–non-conforming clusters can be generated that are more substitutionally active, in contrast to the substitutionally inert Fe_6^{2-} cluster. For example, our recent report elucidated guidelines for cluster coordination of electron-starved clusters by multidentate phosphine ligands: single iron site coordination leads to cluster disproportionation, whereas multi-iron site chelation provides intact penta-iron clusters.[14] Applying the same approach we have also investigated substitution with phosphides and most importantly thiolates, leading to a novel thiolate-bound intact hexa-iron carbide cluster $[Fe_6(\mu_6\text{-C})(\mu_2\text{-Stol})(\mu_2\text{-CO})_2(CO)_{14}]^{3-}$.[21] This previous work provides insight into successful routes for substitution reactions on six-iron clusters. In this work, we seek to establish a new platform for investigating downstream ligand/metal substitution reactions.

A previous report from our group utilized molybdenum as a heteroatom for penta-iron-carbide clusters in an $[Fe_5Mo(\mu_6\text{-C})(\mu_2\text{-CO})_3(CO)_{14}]^{2-}$ cluster[22,23] (selected for its nominal relevance to the active site of nitrogenase), and demonstrated the cluster's catalytic activity towards selective reductions of diphenyl acetylene. While previously reported,[24] $[Fe_4Mo_2(\mu_6\text{-C})(\mu_2\text{-CO})_2(CO)_{16}]^{2-}$ ($Fe_4Mo_2^{2-}$, **2**) was not crystallographically characterized. In this work, we synthesize and utilize the novel di-molybdenum iron-carbide cluster $[Fe_4Mo_2(\mu_6\text{-C})(\mu_2\text{-CO})_2(CO)_{16}]^{2-}$ (**2**) to examine its structural parameters and reactivity toward reductions of diphenylacetylene (DPA).

Results & discussion

Synthesis

Synthesis of the di-anionic $[Fe_4(\mu_4\text{-C})(CO)_{12}]^{2-}$ was accomplished through a series known reactions starting from the well-characterized $[Fe_6(\mu_6\text{-C})(\mu_2\text{-CO})_4(CO)_{12}]^{2-}$ cluster (Scheme 1), followed by selective removal of two iron sites using $FeCl_3$ (as an inner-sphere oxidant), thus generating the acetyl(ester)-capped carbide cluster $[Fe_4(\mu_4\text{-C(COOMe)})(CO)_{12}]^-$.[25] This four-iron cluster was protonated with triflic acid to extrude methanol, thus providing the carbide-authentic neutral cluster $[Fe_4(\mu_4\text{-C})(CO)_{13}]$.[25] Subsequent reduction with KC_8 generates the key dianionic intermediate $[Fe_4(\mu_4\text{-C})(CO)_{12}]^{2-}$ (**1**).[25]

In our previous report of the synthesis of the penta-iron $[Fe_5Mo(\mu_6\text{-C})(\mu_2\text{-CO})_3(CO)_{14}]^{2-}$ cluster, addition of a stoichiometric amount of Mo(cycloheptatriene)$(CO)_3$ to the five-iron cluster $[Fe_5(\mu_5\text{-C})(\mu_2\text{-CO})_2(CO)_{12}]^{2-}$ resulted in the formation of the target mono-molybdenum cluster $[Fe_5Mo(\mu_6\text{-C})(\mu_2\text{-CO})_3(CO)_{14}]^{2-}$. In contrast, stoichiometric addition of 1–2 equiv. of Mo(cycloheptatriene)$(CO)_3$ to **1** led only to a mixture of products (postulated from preliminary crystal structure data) that co-crystallized and proved inseparable. Thus, to isolate a pure crystalline sample of $[K(benzo\text{-}18\text{-}c\text{-}6)]_2[Fe_4Mo_2(\mu_6\text{-C})(\mu_2\text{-CO})_2(CO)_{16}]$ (**2**), it proved necessary to perform the reaction with an excess of Mo(chpt)$(CO)_3$ (5 equiv.) and mild heating (80 °C) to drive the reaction to completion.

X-ray structures of 1 & 2

Similar to previous reports on the structure of tetra-iron-carbide clusters,[25] the crystal structure data for **1** (Fig. S3) revealed a four-coordinate carbide encompassed by four Fe atoms fixed in a butterfly geometry. The crystal structure of **2** (Fig. 1) reveals that the core Fe_4 'butterfly' motif remains unchanged from **1**, imposing *cis*-Mo coordination about the carbide. This is expected as there is no CCDC structure for a tetra-iron–heterometal carbide or nitride cluster that does not preserve the Fe_4 butterfly motif. Upon insertion of the two molybdenum centers, the average Fe–Fe bond contract and Fe–$C_{carbide}$ bond lengths become elongated to 2.61(12) Å and 1.91 (4) Å, respectively. A trend in these contacts becomes apparent upon comparing the Fe_6, Fe_5Mo and Fe_4Mo_2 cores (Table 1).

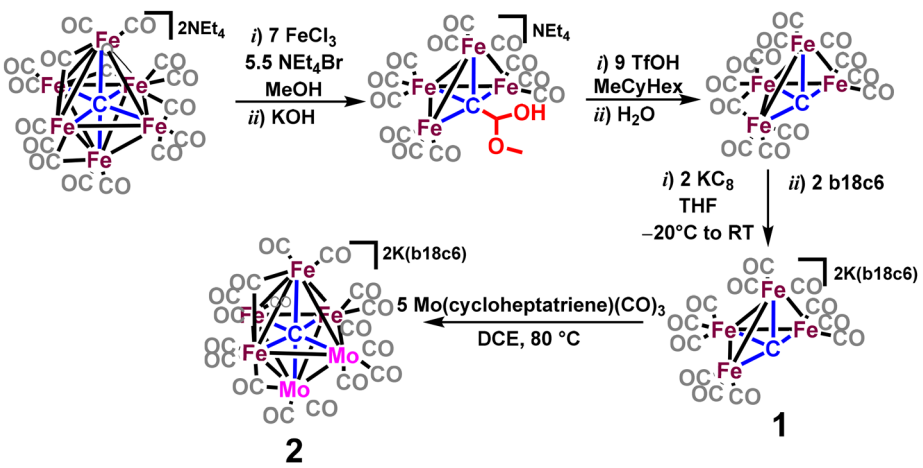

Scheme 1 Synthetic pathway to generate $[K(benzo\text{-}18\text{-}crown\text{-}6)]_2[Fe_4Mo_2(\mu_6\text{-C})(CO)_{16}(\mu_2\text{-CO})_2]$ (**2**).

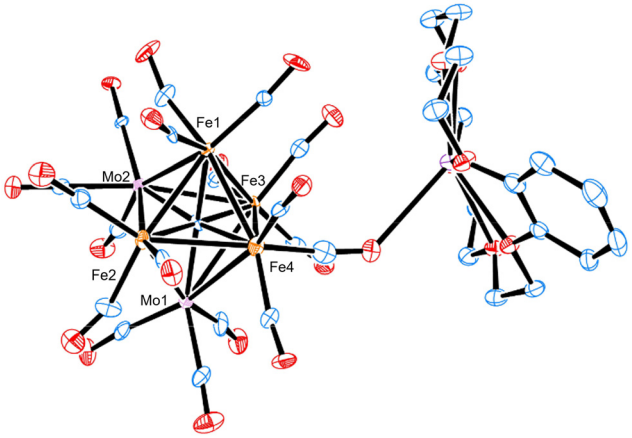

Fig. 1 ORTEP diagram (50% thermal ellipsoids) of **2**. Hydrogens are omitted for clarity. A complete ORTEP diagram of the full asymmetric part of the unit cell is included in SI (Fig. S4).

Table 1 Average metal-carbide and metal–metal bond distances (Å) for $[K(benzo\text{-}18\text{-}crown\text{-}6)]_2[Fe_4(\mu_4\text{-}C)(CO)_{12}]$ (**1**), $(NEt_4)_2[Fe_6(\mu_6\text{-}C)(\mu_2\text{-}CO)_4(CO)_{12}]$,[26] $[K(benzo\text{-}18\text{-}crown\text{-}6)]_2[Fe_5Mo(\mu_6\text{-}C)(\mu_2\text{-}CO)_3(CO)_{14}]$[23] and $[K(benzo\text{-}18\text{-}c\text{-}6)]_2[Fe_4Mo_2(\mu_6\text{-}C)(\mu_2\text{-}CO)_2(CO)_{16}]$ (**2**)

Bond	Fe_4 (**1**)	Fe_6	Fe_5Mo	Fe_4Mo_2 (**2**)
Fe–$C_{carbide}$	1.87 ± 0.11	1.88 ± 0.01	1.90 ± 0.05	1.91 ± 0.04
Fe–Fe	2.62 ± 0.04	2.66 ± 0.06	2.65 ± 0.01	2.61 ± 0.12
Mo–$C_{carbide}$	—	—	2.11 ± 0.06	2.11 ± 0.02
Mo–Fe	—	—	2.91 ± 0.03	2.89 ± 0.05

As Fe atoms are discretely replaced with Mo atoms, the Fe–Fe bonds shorten, while the Fe–$C_{carbide}$ bonds elongate. In contrast to the comparison of Fe_6 and Fe_4 (in which the Fe_4C motif becomes overall compressed), the trend suggests that the presence of the molybdenum atoms promote a displacement of the carbide away from the Fe_4 unit.

Diphenylacetylene reduction

The reactivity of the Fe_4Mo_2 cluster was examined and compared to the iron-only Fe_6 cluster in its activity for the reduction of diphenylacetylene (DPA). A similar reduction of ethyne is reported with the native nitrogenase enzyme and follows literature precedent for the activation of alkynes by iron carbonyls by bonding of the alkyne to the iron centers, enforcing certain conformations leading to enhanced selectivity.[27,28] The reduction of DPA was pursued to provide insight into selective reductions of triply-bonded functional groups. Results are included below in Table 2, for the following general (unbalanced) reaction (Scheme 2).

Initial investigations consisted of control reactions without cluster for each proton source. Sodium perylinide [Na_2(per)] was selected over a stronger reductant (*e.g.* KC_8), as our previous report demonstrated that while stronger reductants lead to increased conversion, they also result in lower selectivity for the *cis*-alkene product; thus, we opted for the reductant that provides greatest selectivity. For the catalyst-free reaction of Na_2(per) with 2,4,6-trimethylanilinium triflate ([Me_3AnH]OTf, Scheme 3) a near-zero conversion of 0.09% was obtained, but with surprising selectivity towards the intermediately reduced diphenylethylene products (no observed diphenylethane), and relatively high selectivity towards the desired *cis* product (0.89 *cis*/*trans*). Upon addition of the Fe_6 cluster under the same conditions, conversion was substantially increased (17.7%), but selectivity was decreased for both alkene/alkane selectivity (1.18) and for *cis*/*trans* selectivity (0.05) compared with the catalyst-free reaction. The novel Fe_4Mo_2 exhibited nearly identical conversion and selectivity as Fe_6, despite the differences in structure. The addition of either cluster as a catalytic unit to these reaction conditions increased conversion while decreasing selectivity, in contrast to previous work with the analogous Fe_5Mo cluster, which resulted in increased conversion and selectivity for the alkene and *cis* products.

Notably, comparison of the same reductions with a more sterically encumbered proton source (2,4,6-tri-*tert*-butylanilinium triflate, [^{t}Bu$_3$AnH]OTf) resulted in a different trend: addition of catalytic Fe_6 resulted in a 5-fold decrease in conversion (15.9% to 2.7%) and a moderate decrease in alkene/alkane selectivity (12.6 to 7.6) yet provided greater selectivity of the *cis versus trans* product (0.01 to 0.22). Fe_4Mo_2 provided a lower conversion (1.5%) than either the iron-only or catalyst-free reactions with a marginally lower selectivity (9.9) for alkene/alkane compared to the catalyst-free reaction (12.6), but with the highest selectivity for the *cis* product observed (0.96 *cis*/*trans*) overall in this report. This trend towards lower conversion but higher selectivity for the *cis*-alkene product is the inverse of the trend observed with the less bulky [Me_3AnH]OTf; however, it does parallel the trend found previously for Fe_5Mo, which also exhibited increased selectivity despite increased overall conversion. Comparison of [Me_3AnH]OTf and [^{t}Bu$_3$AnH]OTf reactions demonstrated the same trend found previously, with the more sterically encumbered proton source resulting in decreased conversion but increased selectivity for the *cis*-alkene product.

Temperature dependence was also investigated, initially with [^{t}Bu$_3$AnH]OTf. At both decreased (−20 °C) and elevated (60 °C) temperature, the selectivity for the *cis* alkene product decreased while selectivity for the alkene product over the alkane product remained similar. At lower temperatures conversion also decreased, however conversion remained unchanged at elevated temperature—in both cases contradictory to our previous work with Fe_5Mo. Interestingly, a different trend emerged with [Me_3AnH]OTf, which exhibited greatly increased selectivity for the *cis* product in the case of both lowered and elevated temperature—despite decreased conversion and selectivity for the alkene product (in both cases).

We also investigated the effect of pK_a by using 2,6-dimethylanilinium triflate ([Me_2AnH]OTf), a proton source with identical steric bulk near the acidic site, but with a lower pK_a due to the absence of the *para* methyl group. The more acidic proton source with Fe_6 provided a remarkable 60.2% conversion—the

Table 2 Selected results from reductions of DPA to *cis*/*trans*-diphenylethylene and diphenylethane

Catalyst	Reductant	Proton source	pK_a	Temp (°C)	Convn (%)	C=C/C–C ratio	*cis*/*trans* ratio
None	Na_2(per)	[Me_3AnH]OTf	4.37	rt	0.09	C=C only	0.89
Fe_6	Na_2(per)	[Me_3AnH]OTf	4.37	rt	17.70	1.18	0.05
Fe_4Mo_2	Na_2(per)	[Me_3AnH]OTf	4.37	rt	16.98	1.09	0.03
Fe_4Mo_2	Na_2(per)	[Me_3AnH]OTf	4.37	−20	0.43	0.22	0.50
Fe_4Mo_2	Na_2(per)	[Me_3AnH]OTf	4.37	60	1.08	0.19	0.95
None	Na_2(per)	[^{t}Bu$_3$AnH]OTf	3.30	rt	15.88	12.58	0.01
Fe_6	Na_2(per)	[^{t}Bu$_3$AnH]OTf	3.30	rt	2.68	7.62	0.22
Fe_4Mo_2	Na_2(per)	[^{t}Bu$_3$AnH]OTf	3.30	rt	1.51	9.95	0.96
Fe_4Mo_2	Na_2(per)	[^{t}Bu$_3$AnH]OTf	3.30	−20	0.27	9.82	0.61
Fe_4Mo_2	Na_2(per)	[^{t}Bu$_3$AnH]OTf	3.30	60	1.20	9.37	0.28
Fe_6	Na_2(per)	[Me_2AnH]OTf	3.95	rt	60.23	1.32	~0
Fe_4Mo_2	Na_2(per)	[Me_2AnH]OTf	3.95	rt	11.84	3.31	0.01

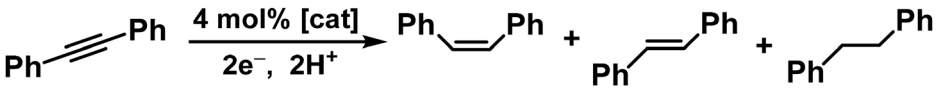

Scheme 2 Reduction of DPA and possible product outcomes.

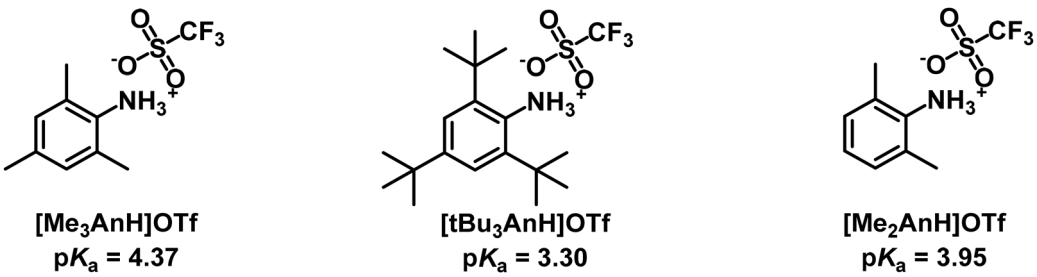

Scheme 3 Anilinium triflate salts used as proton sources, including the pK_a values for the relevant acidic protons.

highest conversion observed in our work with these iron clusters—but providing very poor *cis* and alkene selectivity. Fe_4Mo_2 resulted in decreased conversion, but notably a three-fold increase in alkene selectivity. The seemingly outsized effect of such a small increase in acidity indicates the presence of a barrier to cluster protonation—which once overcome, greatly increases reaction rate. This suggests that the iron-only cluster Fe_6 provides a more accessible protonated state than the Fe_4Mo_2 cluster.

Mechanistic insight from electrochemistry, X-ray photoelectron spectroscopy & ^{1}H NMR

In our previous report we provided evidence that the catalytic method proceeds first *via* two-electron reduction of the cluster to a tetra-anionic cluster followed by subsequent protonation to form a dihydride di-anionic cluster. To ensure this cluster remained intact, IR spectra were collected before and after reduction, showing a shift of an intense feature from 1928 cm^{-1} to 1894 cm^{-1}, consistent with a two electron reduction (Fig. S5). To further implicate a protonated $H_2Fe_4Mo_2^{2-}$ cluster was formed, the IR spectrum was monitored and a blue-shift from 1894 cm^{-1} to 2018 cm^{-1} was observed, consistent with a two-electron oxidation back to a di-anionic species. Evidence of the protonated cluster was also observed in the ^{1}H NMR spectrum after protonation (Fig. 2), exhibiting resonances at δ = −22 and −26 ppm that correspond to bridging hydride and dihydride species respectively—as observed in the analogous (previously reported by Zacchini) reaction of Fe_6 (δ = −21 ppm) or Fe_5Mo (δ = −26 ppm), as well as the recent work with Fe_6^{4-} (δ = −21, −27 ppm for mono- and di-hydride species respectively).[23,29]

In our previous report, we provided evidence that the catalytic mechanism proceeds first *via* two-electron cluster reduction (eqn (1)) followed by protonation to generate a hydride-supported di-anionic cluster (eqn (2)):

$$[M_6]^{2-} + 2e^- \rightarrow [M_6]^{4-} \quad (1)$$

$$[M_6]^{4-} + 2H^+ \rightarrow [H_2M_6]^{2-} \quad (2)$$

$$[H_2M_6]^{2-} + 2e^- \rightarrow [H_2M_6]^{4-} \quad (3)$$

The hydride supported cluster can, itself, directly act upon DPA, or undergo further two-electron reduction to then react with substrate (eqn (3)). Binding of the DPA is theorized to

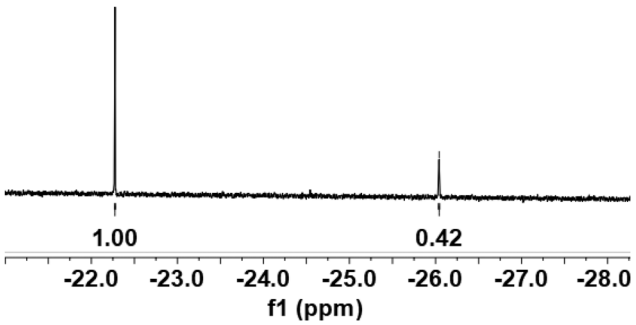

Fig. 2 ^{1}H NMR spectrum (400 MHz, CD_3CN) in the hydride region after reduction and protonation of **2**, indicating the presence of hydride species as the putative catalytic intermediate in the hydrogenation of DPA.

occur analogously to a previous report utilizing iron-carbonyl species with a single iron site binding the DPA π system followed by hydrogenation utilizing cluster bound hydrides.[30] As a control to investigate DPA binding the reduced 4-clusters ^{13}C NMR was collected after reacting Fe_6 with KC_8 and upon addition of DPA the only carbide stretches observed corresponded to the Fe_6^{2-} and Fe_6^{4-} species (δ = 483.71 ppm and 488.89 ppm respectively), consistent with previous work and precluding a DPA bound cluster forming.[31]

Our previous report[32] demonstrated that the Fe_5Mo cluster is an 'electronic hybrid' between Fe_6^{2-} and Fe_5^{2-} clusters, nominally serving as a slightly reduced Fe_5^{2-} cluster capped with a slightly oxidized Mo rather than as an Fe_5Mo^{2-} cluster with even charge distribution. As such, the iron sites in Fe_5Mo^{2-} exhibit an average oxidation state of approximately $Fe^{+0.4}$, with a higher average oxidation state than in the case of the iron-only Fe_6^{2-} ($Fe^{+0.33}$). We thus hypothesize there is a similar, but even more pronounced effect with Fe_4Mo_2: capping the Fe_4^{2-} fragment with two neutral Mo(0) centers promotes access to the most oxidized iron sites in the Fe_xMo_y series, namely (or nominally, at least) as $Fe^{+0.5}$. To test this hypothesis, X-ray photoelectron spectra (XPS) were collected for Fe_6, Fe_5Mo and Fe_4Mo_2 and analyzed in the Fe 2p region (j=3/2 and 1/2) to determine the extent of oxidation at the iron sites (Fig. 3a).[33]

Consistent with our hypothesis, the all-iron Fe_6 cluster demonstrated the lowest average iron oxidation state with an binding energy of 708.05 eV.[34] Upon substitution of iron for an additional molybdenum, an increase in binding energy is observed with Fe_5Mo (708.31 eV) → Fe_4Mo_2 (708.39 eV) indicating a slightly higher average iron oxidation state in each case. Unexpectedly, the difference between Fe_6 and Fe_5Mo is 0.26 eV (attributable to a difference in oxidation state of ~0.07), whereas the nominally more oxidized iron sites in Fe_4Mo_2 differed from Fe_5Mo by only 0.08 eV—despite an expected oxidation state difference of ~0.1.

The corresponding Mo 3d XPS spectra provide insight regarding charge distribution across the clusters (Fig. 3b). Previous work showed that the Mo site in Fe_5Mo is slightly oxidized, and this work further supports that conclusion with an Fe_5Mo Mo 3d binding energy of 228.18 eV compared to literature Mo(0) of 228.0 eV.[32,35] Interestingly, the Fe_4Mo_2 cluster exhibits further oxidized Mo sites (228.29 eV) and provides insight regarding the small shift in Fe 2p features in the Fe_4Mo_2 XPS spectrum (Fig. 3a): namely, that the iron sites do not exhibit proportionally higher binding energy features (*i.e.* average oxidation state does not increase as much as expected) as the two Mo(0) sites experience some loss of electron density in Fe_4Mo_2, compared with an invariant Mo(0)-'like' oxidation state in the Fe_5Mo cluster. Despite this, Fe_4Mo_2 still exhibits the highest energy Fe 2p binding energies (proxy for most oxidized iron sites), and it would thus be expected for the cluster to exhibit reactivity similar to the 'free' (uncapped) Fe_4 unit.

This is notable as the protonated Fe_4^{2-} was crystallographically characterized[36]; however, protonation results in one Fe–H–Fe bridging hydride and one carbide-based C–H 'protonation' in $HFe_4(\eta^2\text{-CH})(CO)_{12}$; this cluster is readily deprotonated and has limited stability in solution. However, further and/or

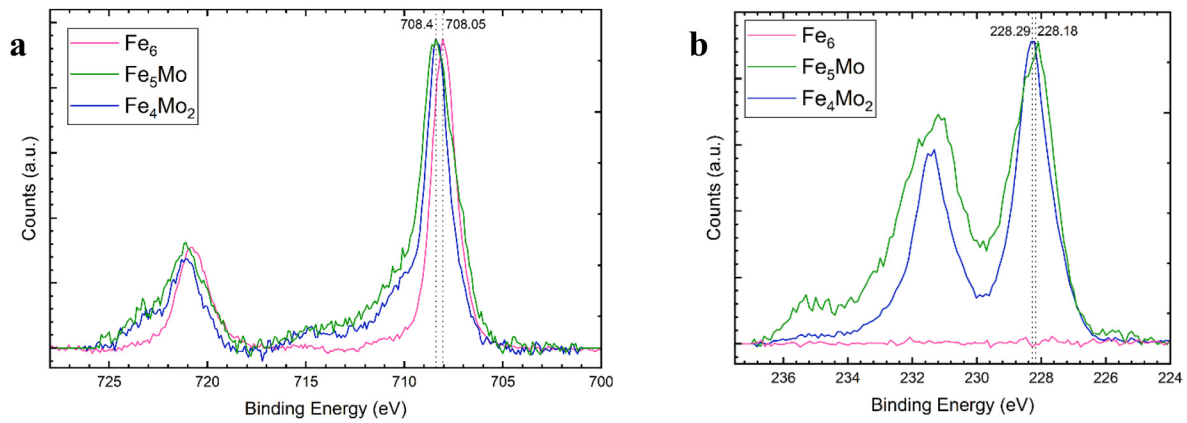

Fig. 3 High-resolution X-ray photoelectron spectrum (XPS) of (a) the iron 2p region and (b) the molybdenum 3d region: pink, Fe_6; green, Fe_5Mo; blue, Fe_4Mo_2.

excess acid treatment results in carbide protonation (eventually released as CH_4), thus precluding the 'bare' Fe_4 cluster's efficacy as a reduction catalyst.[37] In contrast, the Mo_2-capped Fe_4 unit in **2** in this work serves as an 'inorganic protecting group', preventing carbide protonation and driving the formation of an exclusively metal-based (no carbide protonation) dihydride intermediate, overall producing a catalytically competent species.

Overall, the XPS data indicate that Mo substituted clusters with fewer iron sites have higher average oxidation states, thus resulting in more tightly bound hydrides (compared with Fe_6 or Fe_5Mo) and rendering reactivity more selective. The catalysis results above (Table 2) also indicate that the barrier to protonation for Fe_4Mo_2 is important, with less sterically hindered proton sources evidently overcoming the barrier and 'over-protonating' the cluster, thus resulting in more reactive but less selective hydride intermediates. Alternatively, more sterically hindered proton sources evidently 'under-protonate' the cluster leading to less reactive but more selective substrate conversions.

Cyclic voltammetry data was also collected was collected for Fe_6, Fe_5Mo and Fe_4Mo_2 to provide further insight into the reduction and oxidation potentials of the clusters—and possible accessibility of the two-electron reduced cluster intermediates (Fig. 4 and SI Fig. S10–20). Consistent with previous work by Zacchini *et al.*, the Fe_6 cluster showed multiple and poorly resolved redox features corresponding to the formation of Fe_6^{4-} and subsequent re-oxidation back to Fe_6^{2-}; similar features were observed for Fe_5Mo, albeit at slightly higher potentials. However in the case of Fe_4Mo_2, the highest oxidation potential in the series is obtained—consistent with the oxidation of more electropositive iron centers in Fe_4Mo_2 relative to Fe_6 and Fe_5Mo. This observation further supports assignment of higher average oxidation state iron sites in the Fe_4Mo_2 cluster.

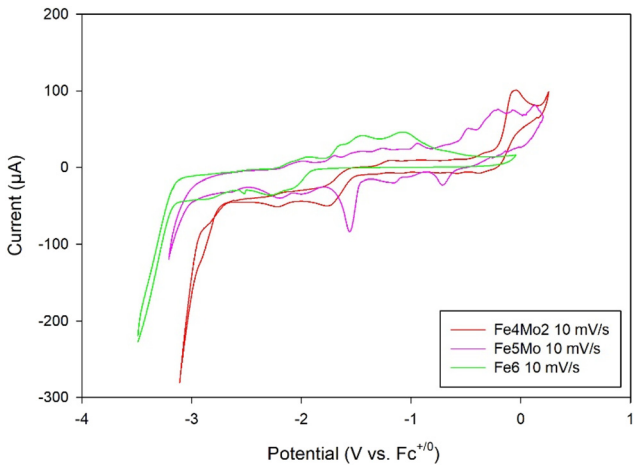

Fig. 4 Comparison of cyclic voltammograms (*vs.* Fc/Fc^+) of 5 mM of cluster in MeCN containing 0.2 M $TBAPF_6$. Experiment conditions: WE, glassy carbon; CE, Pt wire; RE, Ag wire quasi-reference; scan rate: 10 mV s^{-1}.

Conclusion

In summary, we report a synthetic route to the structurally characterized iron-dimolybdenum carbide cluster $[K(benzo\text{-}18\text{-}crown\text{-}6)]_2[(\mu_6\text{-}C)Fe_4Mo_2(\mu_2\text{-}CO)_2(CO)_{16}]$ (**2**) by addition of Mo (0) centers to a reduced four-iron carbide cluster (**1**), wherein the Fe_4 skeleton retains its 'butterfly' motif and enforces *cis*-Mo_2 coordination about the carbide. The carbide is structurally displaced relative to the starting Fe_4 framework and is contracted towards the Mo sites. Reduction/protonation of **2** affords a cluster-di/hydride species that provides enhanced selectivity for regioselective partial reduction of DPA to *cis*-diphenylethylene product due to increased stability of higher valent iron-hydride species, thus decreasing conversion but enhancing selectivity. Future work will investigate substitution of the strong field carbonyl ligand environment for Fe_mMo_n clusters with for more biologically relevant sulfur-based supports such as thiolates and sulfides (or phosphine/phosphide) through our recently developed *in situ*, outer-sphere oxidation method that renders clusters substitutionally active due to their non-PSEPT (Wade–Mingos rules) electron count.[14,21] We expect that the capping effect of the molybdenum sites will provide an increased extent of sulfide/thiolate (or phosphine/phosphide) substitution compared with iron-only clusters by promoting external L- and X-type ligand binding to the more electropositive (higher average oxidation state) Fe_4 iron centers.

Conflicts of interest

There are no conflicts to declare.

Data availability

The data supporting this article have been included as part of the supplementary information (SI). Supplementary information: additional NMR, IR, XPS, cyclic voltammetry and X-ray structures. See DOI: https://doi.org/10.1039/d6dt00524a.

CCDC 2440297 (**2**) and 2440298 (**1**) contain the supplementary crystallographic data for this paper.[38a,b]

Acknowledgements

We acknowledge the National Science Foundation (CHE-2109175) and the Robert A. Welch Foundation (F-1822) for support of this work. We acknowledge use of a Bruker AVIII HD 500 with Prodigy liquid N_2 Cryoprobe supported by NIH Grant S10 OD021508. EJD acknowledges a University of Texas at Austin, College of Natural Sciences Dean's Strategic Fellowship. We also thank Dr Ian Riddington for his assistance with the collection of GC-MS data for product characterization and Dr Hugo Celio and Jeremy Brinker for their assistance with the collection of XPS data.

References

1 M. A. Beno, J. M. Williams, M. Tachikawa and E. L. Muetterties, Fischer-Tropsch Chemistry: Structure of a Seminal η^2-CH Cluster Derivative, $HFe_4(\eta^2\text{-}CH)(CO)_{12}$, *J. Am. Chem. Soc.*, 1980, **102**(13), 4542–4544, DOI: 10.1021/ja00533a052.

2 M. A. Beno, J. M. Williams, M. Tachikawa and E. L. Muetterties, A Closed Three-Center Carbon-Hydrogen-Metal Interaction. A Neutron Diffraction Study of $HFe_4(\eta^2\text{-}CH)(CO)_{12}$, *J. Am. Chem. Soc.*, 1981, **103**(6), 1485–1492, DOI: 10.1021/ja00396a032.

3 J. H. Davis, M. A. Beno, J. M. Williams, J. Zimmie, M. Tachikawa and E. L. Muetterties, Structure and Chemistry of a Metal Cluster with a Four-Coordinate Carbide Carbon Atom, *Proc. Natl. Acad. Sci. U. S. A.*, 1981, **78**(2), 668–671.

4 S. Ghosh, K. B. Holt, S. E. Kabir, M. G. Richmond and G. Hogarth, Electrocatalytic Proton Reduction Catalysed by the Low-Valent Tetrairon-Oxo Cluster $[Fe_4(CO)_{10}(\kappa^2\text{-dppn})(\mu_4\text{-O})]^{2-}$ [dppn = 1,1′-bis(diphenylphosphino)naphthalene], *Dalton Trans.*, 2015, **44**(11), 5160–5169, DOI: 10.1039/C4DT03323J.

5 I. Čorić and P. L. Holland, Insight into the Iron–Molybdenum Cofactor of Nitrogenase from Synthetic Iron Complexes with Sulfur, Carbon, and Hydride Ligands, *J. Am. Chem. Soc.*, 2016, **138**(23), 7200–7211, DOI: 10.1021/jacs.6b00747.

6 E. M. Holt, K. H. Whitmire and D. F. Shriver, The Role of Metal Cluster Interactions in the Proton-Induced Reduction of CO. the Crystal Structures of [PPN]$\{HFe_4(CO)_{12}\}$ and $HFe_4(CO)_{12}(\eta\text{-}COCH_3)$, *J. Organomet. Chem.*, 1981, **213**(1), 125–137, DOI: 10.1016/S0022-328X(00)93954-8.

7 A. Taheri and L. A. Berben, Tailoring Electrocatalysts for Selective CO_2 or H^+ Reduction: Iron Carbonyl Clusters as a Case Study, *Inorg. Chem.*, 2016, **55**(2), 378–385, DOI: 10.1021/acs.inorgchem.5b02293.

8 K. M. Lancaster, M. Roemelt, P. Ettenhuber, Y. Hu, M. W. Ribbe, F. Neese, U. Bergmann and S. DeBeer, X-Ray Emission Spectroscopy Evidences a Central Carbon in the Nitrogenase Iron-Molybdenum Cofactor, *Science*, 2011, **334**(6058), 974–977, DOI: 10.1126/science.1206445.

9 M. U. Delgado-Jaime, B. R. Dible, K. P. Chiang, W. W. Brennessel, U. Bergmann, P. L. Holland and S. DeBeer, Identification of a Single Light Atom within a Multinuclear Metal Cluster Using Valence-to-Core X-Ray Emission Spectroscopy, *Inorg. Chem.*, 2011, **50**(21), 10709–10717, DOI: 10.1021/ic201173j.

10 C. Joseph, J. P. Shupp, C. R. Cobb and M. J. Rose, Construction of Synthetic Models for Nitrogenase-Relevant NifB Biogenesis Intermediates and Iron-Carbide-Sulfide Clusters, *Catalysts*, 2020, **10**(11), 1317, DOI: 10.3390/catal10111317.

11 J. S. Bradley, G. B. Ansell and E. W. Hill, Homogeneous Carbon Monoxide Hydrogenation on Multiple Sites: A Dissociative Pathway to Oxygenates, *J. Am. Chem. Soc.*, 1979, **101**(24), 7417–7419, DOI: 10.1021/ja00518a055.

12 S. Deabate, P. J. King and E. Sappa, Activation of Carbon Monoxide, Water, and Alcohols on Metal Carbonyl Clusters. Homogeneous and Surface–Mediated Reactions, in *Metal Clusters in Chemistry*, ed. P. Braunstein, L. A. Oro and P. R. Raithby, Wiley, 1999, pp 796–843. DOI: 10.1002/9783527618316.ch2h.

13 J. W. Kolis, F. Basolo and D. F. Shriver, Reactivity of Metal Carbide Clusters: Alkylation and Protonation of [Fe5(CO)14C]2-, *J. Am. Chem. Soc.*, 1982, **104**(21), 5626–5630, DOI: 10.1021/ja00385a011.

14 C. R. Cobb, R. K. Ngo, E. J. Dick, V. M. Lynch and M. J. Rose, Multi-Phosphine-Chelated Iron-Carbide Clusters via Redox-Promoted Ligand Exchange on an Inert Hexa-Iron-Carbide Carbonyl Cluster, $[Fe_6(\mu_6\text{-C})(\mu_2\text{-CO})_4(CO)_{12}]^{2-}$, *Chem. Sci.*, 2024, **15**(29), 11455–11471, DOI: 10.1039/D4SC01370K.

15 S. Saha, L. Zhu and B. Captain, Synthesis and Structural Characterization of Bimetallic Iron–Nickel Carbido Cluster Complexes, *Inorg. Chem.*, 2010, **49**(7), 3465–3472, DOI: 10.1021/ic100057x.

16 C. Femoni, R. D. Pergola, M. C. Iapalucci, F. Kaswalder, M. Riccò and S. Zacchini, Copolymerization of $Fe_4Cu_2C(CO)_{12}$ Moieties with Bidentate N-Ligands: Synthesis and Crystal Structure of the $[Fe_4Cu_2(\mu_6\text{-C})(CO)_{12}(\mu\text{-Bipy})]_4\cdot 8THF$ Square Tetramer and the Infinite $[Fe_4Cu_2(\mu_6\text{-C})(CO)_{12}(\mu\text{-L–L})]_\infty$ Zigzag Chains, *Dalton Trans.*, 2009,)(No. 9), 1509–1511, DOI: 10.1039/B821639H.

17 R. Della Pergola, A. Sironi, L. Garlaschelli, D. Strumolo, C. Manassero, M. Manassero, S. Fedi, P. Zanello, F. Kaswalder and S. Zacchini, Fe–Cu Octahedral Carbide Clusters, and the Replacement of Their Labile Halide Ligands: Synthesis, Solid State Structure, Substitution and Electrochemical Reactivity of $[Fe_5C(CO)_{14}(CuBr)]^{2-}$, $[Fe_4C(CO)_{12}(CuCl)_2]^{2-}$, $[\{Fe_4Cu_2C(CO)_{12}(\mu\text{-Cl})\}_2]^{2-}$, $[Fe_5C(CO)_{14}(CuOC_4H_8)]^-$ and $[Fe_4C(CO)_{12}(CuNCMe)_2]$, *Inorg. Chim. Acta*, 2010, **363**(3), 586–594, DOI: 10.1016/j.ica.2009.01.025.

18 L. A. Polyakova, S. P. Gubin, A. Churakov and L. G. Kuz'mina, $[Fe_3(\mu_3\text{-O})(CO)_9]^{2-}$, Dianion as a Suitable Material for the Preparation of Homo- and Heterometallic Carbonyl Clusters, *Russ. J. Coord. Chem.*, 1999, **25**, 711–720.

19 B. F. G. Johnson, D. A. Kaner, J. Lewis, P. R. Raithby and M. J. Rosales, Syntheses and Structural Characterisations of Some Novel Mixed-Metal Iron-Gold Carbido Clusters; X-Ray Crystal Structures of Fe4AuC(η-H)(CO)12(PPh3) and Fe4Au2C(CO)12(PEt3)2, *J. Organomet. Chem.*, 1982, **231**(3), C59–C64, DOI: 10.1016/S0022-328X(00)92900-0.

20 C. Joseph, C. R. Cobb and M. J. Rose, Single–Step Sulfur Insertions into Iron Carbide Carbonyl Clusters: Unlocking the Synthetic Door to FeMoco Analogues, *Angew. Chem.*, 2021, **133**(7), 3475–3479, DOI: 10.1002/ange.202011517.

21 C. R. Cobb, R. K. Ngo, S. Vasylevskyi, Y. Hur, E. J. Dick, J. A. Balderas and M. J. Rose, Single-Step Access to Thiolate-Supported, Six-Iron Clusters with an Authentic

Carbide: Synthesis of $[Fe_6(\mu_6\text{-}C)(\mu_2\text{-}Stol)(\mu_2\text{-}CO)_2(CO)_{12}]^{3-}$ via Non-PSEPT, Redox Intermediates, *Inorg. Chem.*, 2025, **64**(33), 16734–16746 https://doi.org/10.1021/acs.inorgchem.4c05362.

22 M. Tachikawa, A. C. Sievert, E. L. Muetterties, M. R. Thompson, C. S. Day and V. W. Day, Metal Clusters., 24. Synthesis and Structure of Heteronuclear Metal Carbide Clusters, *J. Am. Chem. Soc.*, 1980, **102**(5), 1725–1727, DOI: 10.1021/ja00525a047.

23 C. Joseph, S. Kuppuswamy, V. M. Lynch and M. J. Rose, Fe 5 Mo Cluster with Iron-Carbide and Molybdenum-Carbide Bonding Motifs: Structure and Selective Alkyne Reductions, *Inorg. Chem.*, 2018, **57**(1), 20–23, DOI: 10.1021/acs.inorgchem.7b02615.

24 M. Tachikawa, R. L. Geerts and E. L. Muetterties, Metal Carbide Clusters Synthesis Systematics for Heteronuclear Species, *J. Organomet. Chem.*, 1981, **213**(1), 11–24, DOI: 10.1016/S0022-328X(00)93947-0.

25 J. S. Bradley and E. W. Randall, Carbidocarbonyl Clusters of Iron [and Discussion], *Philos. Trans. R. Soc., A*, 1982, **308**(1501), 103–113.

26 S. Kuppuswamy, J. D. Wofford, C. Joseph, Z. Xie, A. K. Ali, V. M. Lynch, P. A. Lindahl and M. J. Rose, Structures, Interconversions, and Spectroscopy of Iron Carbonyl Clusters with an Interstitial Carbide: Localized Metal Center Reduction by Overall Cluster Oxidation, *Inorg. Chem.*, 2017, **56**(10), 5998–6012, DOI: 10.1021/acs.inorgchem.7b00741.

27 J. M. Rivera-Ortiz and R. H. Burris, Interactions among Substrates and Inhibitors of Nitrogenase, *J. Bacteriol.*, 1975, **123**(2), 537–545.

28 A. C. Filippou and T. Rosenauer, A Reaction Pathway of $[Fe(CO)_5]$ with Alkynes via Ferrabicyclobutenones, *Angew. Chem., Int. Ed.*, 2002, **41**(13), 2393–2396, DOI: 10.1002/1521-3773(20020703)41:13%253C2393::AID-ANIE2393%253E3.0.CO;2-3.

29 M. Bortoluzzi, I. Ciabatti, C. Cesari, C. Femoni, M. C. Iapalucci and S. Zacchini, Synthesis of the Highly Reduced $[Fe_6C(CO)_{15}]^{4-}$ Carbonyl Carbide Cluster and Its Reactions with H^+ and $[Au(PPh_3)]^+$, *Eur. J. Inorg. Chem.*, 2017, **2017**(25), 3135–3143, DOI: 10.1002/ejic.201700169.

30 M. Haberberger and S. Enthaler, Straightforward Iron-Catalyzed Synthesis of Vinylboronates by the Hydroboration of Alkynes, *Chem. – Asian J.*, 2013, **8**(1), 50–54, DOI: 10.1002/asia.201200931.

31 L. Liu, T. B. Rauchfuss and T. J. Woods, Iron Carbide-Sulfide Carbonyl Clusters, *Inorg. Chem.*, 2019, **58**(13), 8271–8274.

32 J. McGale, G. E. Cutsail, C. Joseph, M. J. Rose and S. DeBeer, Spectroscopic X-Ray and Mössbauer Characterization of M_6 and M_5 Iron(Molybdenum)-Carbonyl Carbide Clusters: High Carbide-Iron Covalency Enhances Local Iron Site Electron Density Despite Cluster Oxidation, *Inorg. Chem.*, 2019, **58**(19), 12918–12932, DOI: 10.1021/acs.inorgchem.9b01870.

33 G. Beamson, B. T. Pickup, W. Li and S.-M. Mai, XPS Studies of Chain Conformation in PEG, PTrMO, and PTMG Linear Polyethers, *J. Phys. Chem. B*, 2000, **104**(12), 2656–2672, DOI: 10.1021/jp9905629.

34 B. A. Sosinsky, N. Norem and J. Shelly, Spectroscopic Study of a Series of Iron Carbido Clusters, *Inorg. Chem.*, 1982, **21**(1), 348–356, DOI: 10.1021/ic00131a063.

35 C. L. Bianchi, M. G. Cattania and P. Villa, XPS Characterization of Ni and Mo Oxides before and after "in Situ" Treatments, *Appl. Surf. Sci.*, 1993, **70–71**, 211–216, DOI: 10.1016/0169-4332(93)90429-F.

36 M. Tachikawa and E. L. Muetterties, Metal Clusters. 25. A Uniquely Bonded C-H Group and Reactivity of a Low-Coordinate Carbidic Carbon Atom, *J. Am. Chem. Soc.*, 1980, **102**(13), 4541–4542 https://doi.org/10.1021/ja00533a051.

37 S. Deabate, P. J. King and E. Sappa, Activation of Carbon Monoxide, Water, and Alcohols on Metal Carbonyl Clusters. Homogeneous and Surface–Mediated Reactions, in *Metal Clusters in Chemistry*, ed. P. Braunstein, L. A. Oro and P. R. Raithby, Wiley, 1999, pp. 796–843. DOI: 10.1002/9783527618316.ch2h.

38 (*a*) CCDC 2440297: Experimental Crystal Structure Determination, 2026, DOI: 10.5517/ccdc.csd.cc2mxb85; (*b*) CCDC 2440298: Experimental Crystal Structure Determination, 2026, DOI: 10.5517/ccdc.csd.cc2mxb96.